WILEY | Hindawi

Research Article

A Dual Fractal Poroelastic Model for Characterizing Fluid Flow in Fractured Coal Masses

Guannan Liu,[1,2,3] **Dayu Ye,**[3] **Feng Gao** [2,3] **and Jishan Liu**[4]

[1]*Laboratory of Mine Cooling and Coal-Heat Integrated Exploitation, China University of Mining and Technology, Xuzhou, Jiangsu 221116, China*
[2]*State Key Laboratory for Geomechanics and Deep Underground Engineering, China University of Mining and Technology, Xuzhou, Jiangsu 221116, China*
[3]*Mechanics and Civil Engineering Institute, China University of Mining and Technology, Xuzhou City, Jiangsu Province 221116, China*
[4]*Department of Chemical Engineering, School of Engineering, The University of Western Australia, WA 6009, Australia*

Correspondence should be addressed to Feng Gao; fgao@cumt.edu.cn

In the process of coalbed methane exploitation, the fracture and pore structure is the key problem that affects the permeability of coalbed. At present, the coupling effect of fracture and pore structure and in situ stress is seldom considered in the study of coal seam permeability. In this paper, the fractal seepage model is coupled with coal deformation, and the adsorption expansion effect is considered. A multifield coupling model considering the influence of matrix and fracture structure is established. Then, the influence of pore structure parameters of main fracture on macropermeability is analyzed, including (1) fractal dimension of fracture length, (2) maximum fracture length, (3) fractal dimension of throat diameter, and (4) fractal dimension of throat bending. At the same time, the simulation results are compared with the results of Darcy's uniform permeability model. The results show that the permeability calculated by the proposed model is significantly different from that calculated by the traditional cubic model. Under the action of in situ stress, when the porosity and other parameters remain unchanged, the macropermeability of coal is in direct proportion to the fractal dimension of coal fracture length, the fractal dimension of throat diameter, and the maximum fracture length and in inverse proportion to the fractal dimension of coal throat curvature.

1. Introduction

Coalbed methane is one of the main high-quality clean energy sources in the world. In the process of coalbed methane extraction, the fracture and pore network of coal seam is the main space of its migration [1, 2]. Quantitative analysis of the influence of fracture pore structure of coal seam on the macropermeability is the key to improve the extraction rate of coalbed methane and ensure the safety of production [3–5].

The fracture network of coal is highly complex [6–8]. In recent years, researchers have found that a large number of coal and coal fractures have fractal characteristics. In nature, the distribution, length, opening, and orientation of fractures are often random and disordered. It is a great challenge to find its analytical solution. Fractal geometry theory has successfully studied the percolation, heat, and electric conduction of fluids in porous media, as well as the physical quantities related to the roughness of porous media surface, nanofluids, pool boiling, and dendriform bifurcation network [9–11]. Fractal geometry is considered as an effective method to quantitatively describe the structure of fracture network.

Combined with the first law of thermodynamics and fractal description, Deinert et al. [12, 13] simplified the force balance analysis process of capillary force. And the relationship between capillary force and saturation is established by introducing pore volume and fractal dimension of pore surface. Xu et al. [14–16] analyzed the percolation and heat conduction properties of bifurcated tree networks based on

fractal geometry. The bifurcated tree network is an ideal symmetric network, which is very similar to the actual tree branching network in structure. Ishibashi et al. [17] used fractal theory to systematically study the flow characteristics and opening of fractures under different pressures. The results show that the contact area depends on the fracture opening; the fracture permeability meets the power law distribution. By introducing the fractal dimension of pore space, Costa [18] obtained the relationship between Kozeny-Carman equation constant and fractal permeability and porosity. Guarracino [19] established the fracture network permeability model by using the Sierpinski blanket fractal model and predicted the conductivity of hydraulic fracturing. Miao et al. [20–22] extended the theory of fractal porous media to fracture network and established the fractal model of fracture network and dual porous media, discussing the influence of fracture length fractal dimension, pore throat tortuosity fractal dimension, and other structural parameters on permeability. Based on the fractal theory, Wu [23] et al. obtained the expansion deformation of double porosity coal and the nonuniform expansion deformation caused by the pore distribution. Denis et al. [24] observed the deformation of coal after two months of injecting carbon dioxide with a pressure of 3.8 MPa and found that the average deformation of coal is 0.34%.

However, the above research method did not take into account the influence of in situ stress and gas adsorption and desorption phenomenon, which may cause deformation of coal body and change the permeability of coal seam. Therefore, based on fractal permeability models, we establish a multifield coupling model of single porosity seepage [25]. In this work, we extend the coupling model of fractal seepage to dual porosity. The influence of structure parameters on seepage is analyzed: (1) fractal dimension of fracture length, (2) maximum fracture length, (3) fractal dimension of pore diameter, and (4) fractal dimension of tortuosity.

2. Governing Equations

The fractal permeability model is deduced by considering the structural parameters and coupling them with the gas seepage model of adsorption deformation. In order to simplify the calculation of partial differential equations, we make the following assumptions [26]:

(1) Coal deformation satisfies linear elasticity

(2) The influence of heterogeneity and anisotropy is not considered

(3) The adsorption deformation is small

(4) The viscosity of gas is a constant

(5) The gas in the pores is saturated

(6) All streams of flow are in parallel and unmixed layers

2.1. Governing Equations of Gas Flow. It is well known that coal seam resource storage can be divided into adsorption

and free phases according to the existing state, in which the total quality governing equation can be expressed as [23]

$$m_m = \rho_{gm}\phi_m + \rho_{ga}\rho_c \frac{V_L p_m}{p_m + P_L}, \tag{1}$$

$$m_f = \rho_{gf}\phi_f + \rho_{ga}\rho_c \frac{V_L p_f}{p_f + P_L}, \tag{2}$$

where the mass of gases in matrix and fracture is expressed by m_m and m_f and gas density is ρ_{gm} and ρ_{gf}. ρ_{ga} is the gas density under standard conditions; ρ_c is the coal density.

According to the of conservation of mass, the equation of gas quality control can be expressed as

$$\frac{\partial m}{\partial t} + \nabla \cdot \left(\rho_g q_g\right) = Q_s, \tag{3}$$

where t is the total time, ρ_g is the gas density, and q_g is the velocity of Darcy flow. We neglect the effect of gravity on the whole; the flow rate of Darcy flow can be expressed as follows:

$$\dot{q}_g = -\frac{k}{\mu}\nabla p. \tag{4}$$

In Equation (4), $\dot{q}_g$ is the derivative of q_g. The simultaneous formula Equations (1), (2), (3), and (4) shows that the mass conservation equation of gases can be expressed as follows:

$$\left[\phi_m + \frac{\rho_c p_a V_L P_L}{(p_m + P_L)^2}\right]\frac{\partial p_m}{\partial t} + p_m\frac{\partial \phi_m}{\partial t} - \nabla \cdot \left(\frac{k_m}{\mu}p_m\nabla p_m\right) = Q_s,$$

$$\left[\phi_f + \frac{\rho_c p_a V_L P_L}{\left(p_f + P_L\right)^2}\right]\frac{\partial p_f}{\partial t} + p_f\frac{\partial \phi_f}{\partial t} - \nabla \cdot \left(\frac{k_f}{\mu}p_f\nabla p_f\right) = -Q_s,$$

$$\tag{5}$$

where p_a is atmospheric pressure, $p_a = 101.325\,\text{kPa}$.

2.2. Governing Equations of Coal Deformation. Based on the assumption at the beginning of this chapter, we can simplify the relationship between strain and displacement into the following equation [27]:

$$\varepsilon_{ij} = \frac{1}{2}\left(u_{i,j} + u_{j,i}\right), \tag{6}$$

where ε_{ij} is the component of the total strain in different directions; $u_{i,j}$ and $u_{j,i}$ are the displacement components. Therefore, the deformation equilibrium equation can be expressed as

$$\sigma_{ij} + f_i = 0, \tag{7}$$

where σ_{ij} is the component of the stress tensor and f_i is the component of the force. The relationship between adsorption and induced deformation can be expressed as follows:

$$\varepsilon_{ij} = \frac{1}{2G}\sigma_{ij} - \left(\frac{1}{6G} - \frac{1}{9k}\right)\sigma_{kk}\delta_{ij} + \frac{\alpha}{3K}p\delta_{ij} + \frac{\varepsilon_s}{3}\delta_{ij}, \quad (8)$$

where ε_s is the gas adsorption strain. According to the force element analysis, $\sigma_{kk} = \sigma_{11} + \sigma_{22} + \sigma_{33}$. G is the shear modulus of elasticity. K is the bulk modulus of coal, and there are $K = E/3(1 - 2\nu)$. ν is Poisson's ratio of coal. α is the Biot coefficient, $\alpha = 1 - K/K_s$, where K_s is the bulk modulus of coal particles and δ_{ij} is the Crohneck function.

By simplifying Equation (8) and combining Equations (6) and (7), we can obtain that

$$G_{u_i,kk} + \frac{G}{1 - 2\mu}u_{k,ki} - \alpha p_i - K\varepsilon_{s,i} + f_i = 0. \quad (9)$$

Equation (9) is the governing equation of coal deformation.

2.3. Porosity Model. As a porous medium, the volume of coal can be divided into two parts: pore volume and coal volume. Under the influence of adsorption deformation, the pore structure undergoes corresponding deformation, which satisfies the Langmuir equation [23]:

$$\varepsilon_s = \varepsilon_L \frac{p}{P_L + p}. \quad (10)$$

Therefore, the volume strain equation of coal can be expressed as

$$\frac{\Delta V}{V} = -\frac{1}{K}(\bar{\sigma} - \alpha p) + \varepsilon_s. \quad (11)$$

Thus,

$$\frac{\Delta V_p}{V_p} = -\frac{1}{K_p}\left[\bar{\sigma} - \left(1 - \frac{K_p}{K_s}\right)p\right] + \varepsilon_s, \quad (12)$$

where ε_L is Langmuir's volumetric strain, V_p is the volume of pore in medium coal, V_c is the volume of coal, and $\bar{\sigma}$ is the average stress.

If the strain of coal attracted by the solution is assumed to have the same effect as the pore strain mentioned above, that is,

$$K_p = \frac{\phi}{\alpha}K. \quad (13)$$

At the same time, according to the definition of porosity, we can get the following two equations:

$$\frac{\Delta V}{V} = \frac{\Delta V_c}{V_c} + \frac{\Delta \phi}{1 - \phi}, \quad (14)$$

$$\frac{\Delta V_p}{V_p} = \frac{\Delta V_c}{V_c} + \frac{\Delta \phi}{\phi(1 - \phi)}. \quad (15)$$

Combine Equations (11), (12), (14), and (15), the overall volume strain is 0 in the initial state. We can obtain that porosity can be expressed as

$$\phi = \frac{1}{1 + S}[(1 + S_0)\phi_0 + \alpha(S - S_0)], \quad (16)$$

where $S = \varepsilon_v + (p/K_s) - \varepsilon_s$ and $S_0 = (p_0/K_s) + \varepsilon_L p_0/(p_0 + p_L)$. When $S \ll 1$ and $S_0 \ll 1$, Equation (16) can be simplified as follows:

$$\phi = \phi_0 + \alpha\left[\varepsilon_v + \frac{p - p_0}{K_s} + \frac{\varepsilon_L P_L(p_0 - p)}{(p_0 + P_L)(p + P_L)}\right]. \quad (17)$$

2.4. Fractal Permeability Model. In this section, based on fractal geometry, a coal permeability model considering fracture and microstructure is established. Based on this model, the influence of pore structure on macropermeability in time and space is analyzed.

The fractal dimension of pore throat is a fraction between 1 and 2. With the increase of fractal dimension, the coverage and complexity of pore throat also increase correspondingly. According to the fractal model proposed by Miao et al. [21], the fractal power relation can be expressed as follows:

$$N(\geq \lambda) \propto \lambda^{-D_f}, \quad (18)$$

where λ is the equivalent radius of the pore, $\lambda_{\min} \leq \lambda \leq \lambda_{\max}$. N is the pore number of the object of study. D_f is the fractal dimension of the pore in the region. For two-dimensional object of study, $1 < D_f < 2$. Therefore, Equation (18) can also be rewritten as follows:

$$N(\geq \lambda) = k_c\lambda^{-D_f}. \quad (19)$$

In Equation (19), k_c is a positive proportional coefficient. From Equation (19), it can be concluded that the differential equation for the number of voids in the range of $[\lambda, \lambda + d\lambda]$ is

$$dN(\lambda) = -k_c D_f \lambda^{-D_f-1}d\lambda. \quad (20)$$

Therefore, combined with Equation (20), the regional pore probability density function can be expressed as follows:

$$f(\lambda) = \frac{dN(\lambda)}{N_t d\lambda} = -\frac{k_c}{N_t}D_f\lambda^{-D_f-1}. \quad (21)$$

Among them, N_t is the total number of regional holes. The normalized probability density function can be obtained as follows:

$$-\int_{\lambda_{\min}}^{\lambda_{\max}}\frac{k_c}{N_t}D_f\lambda^{-D_f-1}d\lambda = 1. \quad (22)$$

If $\lambda_{\min} \ll \lambda_{\max}$, Equation (22) can be simplified as follows:

$$k_c = N_t \lambda_{\min}^{D_f}. \tag{23}$$

Meanwhile, natural pore network usually satisfies $\lambda_{\min}/\lambda_{\max} \leq 10^{-2}$. According to the fractal distribution of porous media, the number of pores can be expressed as

$$N_t(\lambda) = \left(\frac{\lambda_{\max}}{\lambda_{\min}}\right)^{D_f}. \tag{24}$$

Combine Equations (23) and (24), we can obtain that

$$k_c = \lambda_{\max}^{D_f}. \tag{25}$$

By substituting Equation (25) into Equation (22), we can obtain that

$$dN(\lambda) = -D_f \lambda_{\max}^{D_f} \lambda^{-D_f - 1} d\lambda. \tag{26}$$

Equation (26) is a fractal power expression of pore size. Yang et al. concluded that the length of throat satisfies the following fractal distribution:

$$L_t(\lambda) = \lambda^{1 - D_T} L_0^{D_T}, \tag{27}$$

where λ is the length of the throat, and $L_t(\lambda)$ is the length of the throat along the flow direction. D_T is the fractal dimension of the throat tortuosity, $1 < D_T < 2$.

According to Mitra et al. [28], the relationship between pore size and fractal dimension is as follows:

$$D_f = 2 - \frac{\ln \phi}{\ln (\lambda_{\min}/\lambda_{\max})}. \tag{28}$$

The velocity in the throat can be calculated by Hagen-Poiseuille formula:

$$q(\lambda) = \frac{\pi}{128} \frac{\Delta P}{L_t(\lambda)} \frac{\lambda^4}{\mu}, \tag{29}$$

where ΔP is the pressure difference between the inlet and outlet of the throat. Combining Equation (27) and (29), we can obtain that the total flow control equation of microthroat is

$$Q = -\int_{\lambda_{\min}}^{\lambda_{\max}} q(\lambda) dN(\lambda)$$
$$= \frac{\pi}{128} \frac{\Delta P}{\mu} \frac{A}{L_0} \frac{L_0^{1-D_T}}{A} \frac{D_f}{3 + D_T - D_f} \lambda_{\max}^{3+D_T} \tag{30}$$
$$\cdot \left[1 - \left(\frac{\lambda_{\min}}{\lambda_{\max}}\right)^{D_f} \left(\frac{\lambda_{\min}}{\lambda_{\max}}\right)^{3+D_T-2D_f}\right].$$

Because the two-dimensional throat pore satisfies $1 < D_T < 2$ and $1 < D_f < 2$, it can be obtained $3 + D_T - 2D_f >$

0. Therefore, we can obtain that $0 < (\lambda_{\min}/\lambda_{\max})^{3+D_T-2D_f} < 1$. So Equation (30) can be simplified to

$$Q = -\int_{\lambda_{\min}}^{\lambda_{\max}} q(\lambda) dN(\lambda) = \frac{\pi}{128} \frac{\Delta P}{\mu} \frac{A}{L_0} \frac{L_0^{1-D_T}}{A} \frac{D_f}{3 + D_T - D_f} \lambda_{\max}^{3+D_T}, \tag{31}$$

where A is the cross-sectional area of the throat. According to Darcy's, we can obtain that

$$Q = \frac{kA}{\mu} \frac{\Delta p}{L_0}. \tag{32}$$

Therefore, the fractal governing equations of pore permeability can be obtained by combining Equations (31) and (32):

$$k = \frac{\mu L_0 Q}{\Delta P A} = \frac{\pi}{128} \frac{L_0^{1-D_T}}{A} \frac{D_f}{3 + D_T - D_f} \lambda_{\max}^{3+D_T}. \tag{33}$$

The cross-sectional area of the matrix element is [23]

$$A_m = \frac{A_p}{\phi_m} = \frac{\pi D_p \lambda_{\max}^2}{4(2 - D_p)} \frac{1 - \phi_m}{\phi_m}. \tag{34}$$

And the probability density of fracture is expressed as

$$\frac{-dN(l)}{N_t} = \frac{k}{N_t} D_f l^{-(D_f+1)} dl. \tag{35}$$

In Equation (35), N_t represents the total number of fracture in the coal. The normalization of probability density function can be obtained as follows:

$$\frac{k}{N_t}\left(l_{\min}^{-D_f} - l_{\max}^{-D_f}\right) = \frac{k}{N_t} \frac{1}{l_{\min}^{D_f}} \left(1 - \left(\frac{l_{\min}}{l_{\max}}\right)^{D_f}\right) = 1. \tag{36}$$

when $l_{\min} \ll l_{\max}$, Equation (36) can be simplified as follows:

$$k = N_f l_{\min}^{D_f}. \tag{37}$$

From Equations (34) and (37), we can obtain that

$$\frac{\beta D_l l_{\max}^2 \left(1 - \phi_f\right)}{(2 - D_f)\phi_f} = n \cdot \frac{\pi D_f \lambda_{\max}^2 (1 - \phi_m)}{4(2 - D_p)\phi_m}. \tag{38}$$

Ignoring the interaction between fluid in the matrix pore and fluid in the fracture network [29], if the flow rate into the fracture wall equals the flow rate out of the
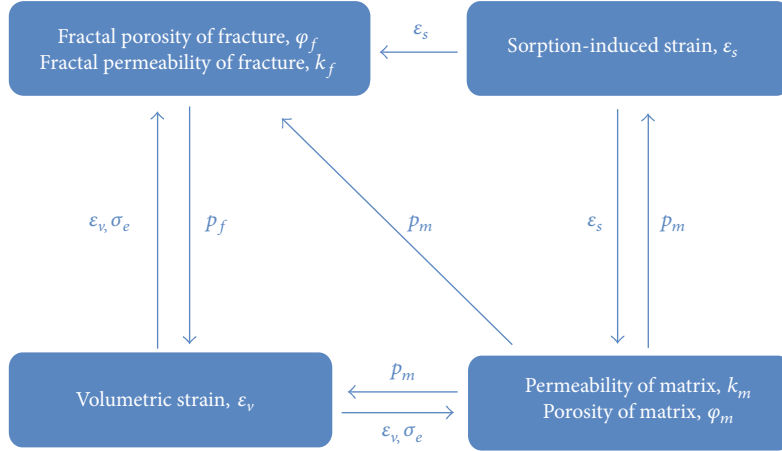
FIGURE 1: Coupling relation of the fractal model.

fracture wall, the total flow rate through the fracture network is as follows:

$$Q = Q_{t,m} + Q_f = n\frac{\pi}{128}\frac{L_0^{1-D_t}}{\mu}\frac{\Delta p}{L_0}\frac{D_p}{3 + D_p - D_T}\lambda_{max}^{3+D_T}$$
$$+ \frac{\beta^3}{12\mu}\frac{D_f\left(1 - \cos^2\alpha\,\sin^2\alpha\right)}{4 - D_f}\frac{\Delta p}{L_0}l_{max}^4. \quad (39)$$

Thus,

$$Q_{t,m} = nQ_m = n\frac{\pi}{128}\frac{L_0^{1-D_t}}{\mu}\frac{\Delta p}{L_0}\frac{D_p}{3 + D_p - D_T}\lambda_{max}^{3+D_T}. \quad (40)$$

By Darcy's law, it can be obtained that

$$Q = \frac{KA_f}{\mu}\frac{\Delta p}{L_0}. \quad (41)$$

Combining Equations (39) and (41), we can obtain that

$$K = \frac{\pi}{128}\frac{L_0^{1-D_t}}{A_m}\frac{D_p}{3 + D_p - D_T}\lambda_{max}^{3+D_T}$$
$$+ \frac{\beta^3}{12A_f}\frac{D_f\left(1 - \cos^2\alpha\,\sin^2\alpha\right)}{4 - D_f}l_{max}^4. \quad (42)$$

Based on the assumption that the coal matrix is impermeable, i.e., satisfies $\phi_m = 0$, therefore, Equation (42) can be simplified as follows:

$$K_f = \frac{\beta^3}{12A_f}\frac{D_f\left(1 - \cos^2\alpha\,\sin^2\alpha\right)}{4 - D_f}l_{max}^4. \quad (43)$$

Equation (43) is the fractal governing equation for fracture permeability. Among them, the permeability of the dynamic permeability fractal model is affected by both

pore and fracture, but the total permeability is not simply the sum of them.

2.5. Mass Transfer between Pores and Fractures. The mass transfer function between the fracture system and the pore system can be expressed as [30]

$$Q = \omega\left(P_m - P_f\right), \quad (44)$$

where $\omega = aV\rho_m(K_m/\mu)$, ρ_m is the volume of gas, and K_m is the permeability of the pore system. μ is the viscosity of fluid, and a is the shape factor of matrix fracture transfer. P_m is the pressure of pore structure, and P_f is the pressure of fracture structure.

In the coupling process of the above physical fields, firstly, the pressure in the volume strain equations is governed by the coal porosity and permeability equations, and the volume stress and volume strain determine the distribution of coal porosity; furthermore, the permeability of the structure-permeability model affects the coal permeability and porosity equations, and the coal porosity on the contrary determines the permeability equations of the structure-permeability model.

Coupling and unification between multiple physical fields are achieved through four parameters: pressure, porosity, strain, and stress. The coupling diagram of the fractal seepage model is shown in Figure 1.

3. Model Validation

In order to verify the correctness of the fractal permeability model established in the preceding section, we apply the fractal permeability models to represent field experimental data [28]. The calculation model is shown in Figure 2, where the pore pressure is 6.2 MPa. The upper boundary is affected by 15 MPa pressure, and the left, right, and lower boundaries are hinged. The ambient pressure is atmospheric pressure, and the left, right, and lower boundaries are no flow. In the simulation of COMSOL Multiphysics, the input parameters are shown in Table 1.
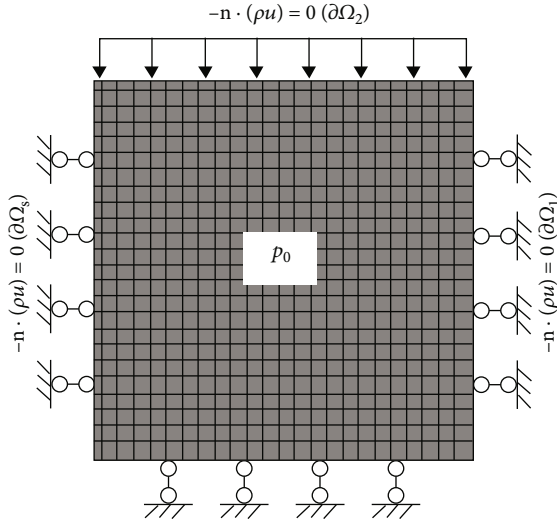
FIGURE 2: Field data verification model.

TABLE 1: Parameters of the simulation model.

Parameter	Value
Young's modulus of coal, $E(\mathrm{MPa})$	2713
Young's modulus of coal grains, $E_s(\mathrm{MPa})$	8139
Poisson's ratio of coal, ν	0.339
Density of coal, $\rho_c\left(\mathrm{kg/m}^3\right)$	1.25×10^3
Density of methane, $\rho_g\left(\mathrm{kg/m}^3\right)$	0.717
Methane dynamic viscosity, $\mu(\mathrm{Pa \cdot s})$	1.84×10^{-5}
Langmuir pressure constant, $P_L(\mathrm{MPa})$	6.109
Langmuir volume constant, $V_L\left(\mathrm{m}^3/\mathrm{kg}\right)$	0.015
Langmuir volumetric strain constant, ε_L	0.02295
Initial porosity of pore system, φ_{m0}	0.00804
Initial porosity of pore system, φ_{f0}	0.02

Considering that the deformation of coal seam caused by the flow field in time and space evolution is nonlinear, COMSOL Multiphysics is used to calculate the coupled equations by the method of multiphysical field coupling. Select the data of field mining under different mines to explore the change of permeability under different pressures. The model fitting results are compared with the experimental data, as shown in Figure 3. From Figure 3, it can be concluded that the proposed structure-gas fractal coupling model is in good agreement with the measured data, which verifies the correctness of the fractal model.

4. Numerical Experiments

4.1. Boundary and Initial Conditions. In order to study the performance of the new model under the influence of coupling multiprocess, we apply the model to a common case: constant confining pressure condition. The calculation
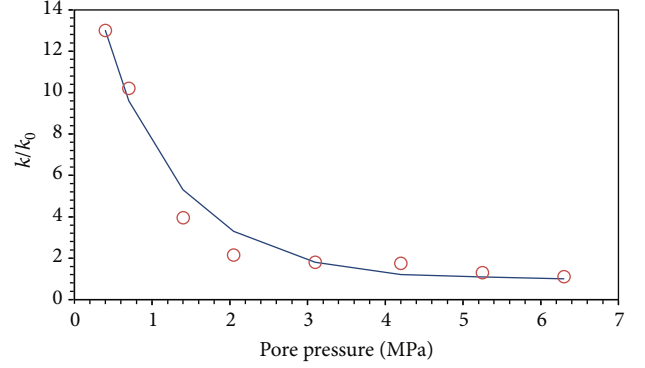

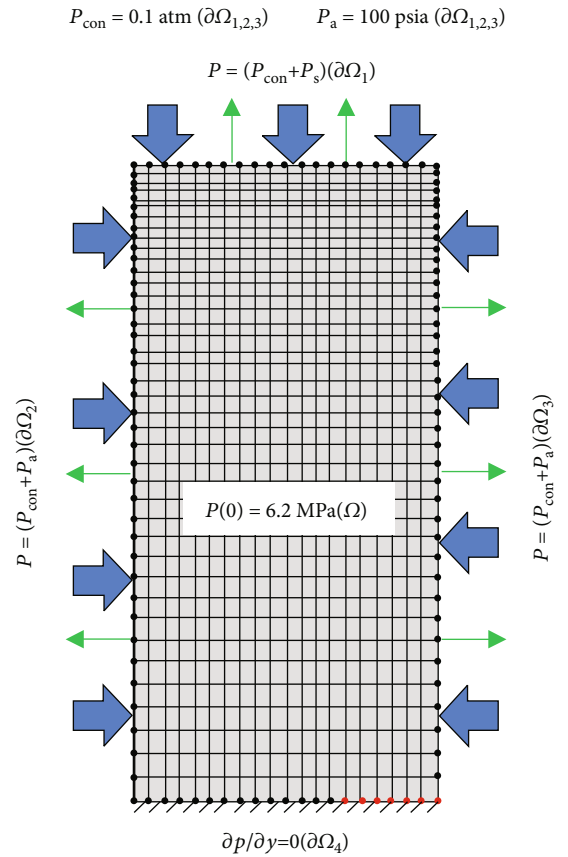FIGURE 3: Comparisons between the calculated results of the model and field data.

FIGURE 4: Schematic diagram of boundary and initial conditions.

model is rectangular, and the size is $0.1\,\mathrm{m} \times 0.05\,\mathrm{m}$. The bottom of the model is constrained by the fixed end, and the rest of the boundary is affected by the pressure of 100 psia. The initial pore pressure of the model is 6.2 Mpa, there is no gas flow at the bottom, and the other three boundary pressures are 0.1 atm. The boundary and initial conditions are shown in Figure 4.

The property parameters of coal and gas are shown in Table 2. Most of the values are derived from previous experimental results [29, 30]; unreported parameters are replaced by contemporary literature.

TABLE 2: Property parameters of coal and gas.

Parameter	Value
Young's modulus of coal, E(MPa)	2713
Young's modulus of coal grains, E_s(MPa)	8139
Poisson's ratio of coal, ν	0.339
Density of coal, ρ_c(kg/m^3)	1.25×10^3
Density of methane, ρ_g(kg/m^3)	0.717
Methane dynamic viscosity, μ(Pa · s)	1.84×10^{-5}
Langmuir pressure constant, P_L(MPa)	6.109
Langmuir volume constant, V_L(m^3/kg)	0.015
Langmuir volumetric strain constant, ε_L	0.02295
Initial porosity of coal, ϕ_0	0.00804
Aperture ratio $\lambda_{\min}/\lambda_{\max}$	0.006
Initial permeability of coal, k_0(m^2)	3.7996×10^{-17}

4.2. Discussion of the Simulation Results

4.2.1. Stress and Deformation Evolution of Coal. Based on the above coupled governing equations and the above parameters, the stress distribution and deformation of coal in 20, 40, 100, and 500 days are simulated. The simulation results are shown in Figure 5.

As shown in Figure 5, with the passage of time, the stress in the central gas-carrying area of coal body increases gradually, and the deformation of coal body increases gradually. The bottom is constrained by the fixed end, and the stress near it is the largest. The stress of the other three boundaries is much smaller than that at the bottom because of the expansion deformation. The minimum stress occurs at the two corners of the top. With the passage of time, the stress at the bottom decreases gradually, while the stress at the left and right edges decreases slowly with the passage of time.

4.2.2. Pressure Evolution of Pore. According to the equation established in this paper and the parameters mentioned above, the distribution of pore pressure in 20, 40, 100, and 500 days is studied. The pore pressure distribution obtained by the model simulation is shown in Figure 6.

From Figure 6, it can be seen that with the passage of time, the pore pressure of coal body decreases as a whole. Because the bottom is constrained by the fixed end and there is no gas flow out, the high-pressure zone finally concentrates on the bottom center. Because the upper, left, and right boundaries have gas flow due to the pressure difference, and the force is not changed, with the passage of time, the low-pressure zone at the edge gradually diffuses to the center. The results of coal body simulation show that the pore pressure decreases gradually from the top, left, and right to the center.

4.2.3. Dynamic Evolution of Permeability in Upper Boundary. Based on this model, the permeability evolution of the fracture and pore system at the upper boundary is studied. With the same model parameters, the evolution of the upper boundary fracture and pore system permeability with time and space is shown in Figures 7 and 8.

From Figures 7 and 8, we can conclude that fracture and pore permeability shows a trend of low edge and high middle permeability at different time. However, with the passage of time, fracture and pore permeability shows a downward trend as a whole. As can be seen from Figures 5 and 6, with the passage of time, the stress of top coal body decreases gradually, and the pore stress decreases gradually. At the same time, the central pressure of coal decreases with the flow of gas, and the permeability of fracture and pore also shows a downward trend with the passage of time.

4.2.4. Effect of Adsorption Strain and Volume Strain on Porosity. The effect of adsorption strain and volume strain on porosity is shown in Figure 9. It can be concluded from the graph that the volume strain and adsorption strain of the matrix have a great influence on the porosity. With the decrease of pore pressure and adsorption pressure, the influence of pore volume strain is not obvious. At the same time, we can conclude that the effect of adsorption-induced volumetric strain is more significant than that of volumetric mechanical volumetric strain.

4.2.5. Evolution of Fractal Dimensions of Fractures and Pores with Time. Meanwhile, based on the above model, we obtained the evolution of fractal dimension of fracture and pore with time. We choose the center point of the model (0.025, 0.05) as the representative point of analysis. We study the evolution of fractal dimension of pore and fracture at this point with time. The evolution of D_f and D_p at this location over time is shown in Figures 10 and 11.

Combining with Figures 10 and 11, we concluded that the evolution curve of fractal dimension in the center of the model decreases with time. Comparing Figures 1 and 11 with Figure 5, the fractal dimension of the model center is proportional to the stress. This is because the stress of coal increases gradually under the action of long-time pressure. As a high-stress area of coal, the longer the compression time, the larger the deformation of pore and fracture structure.

4.2.6. Influence of Adsorption Parameters on Coal Seam Permeability. Based on the model above, we explore the effect of adsorption parameters on coal seam permeability under the condition that other coal seam parameters remain unchanged. We select three points on the axis of the model (0.025, 0.025; 0.025, 0.05; 0.025, 0.075) as the representative points of the analysis. And the simulation results are shown in Figures 12, 13, and 14.

The Langmuir volume constant (V_L) is the maximum adsorption capacity under the condition of pore fracture equilibrium of coal seam. So, as it increases, the volume, number, and surface area of small fractures increases. And the fractal dimension also increases. Langmuir pressure (P_L) is the corresponding pressure when the adsorption capacity reaches half of Langmuir volume (V_L). Because of the increase of Langmuir pressure, micropores and small fractures close; the fractal dimension eventually decreases. Besides, with the increase of Langmuir's volume strain
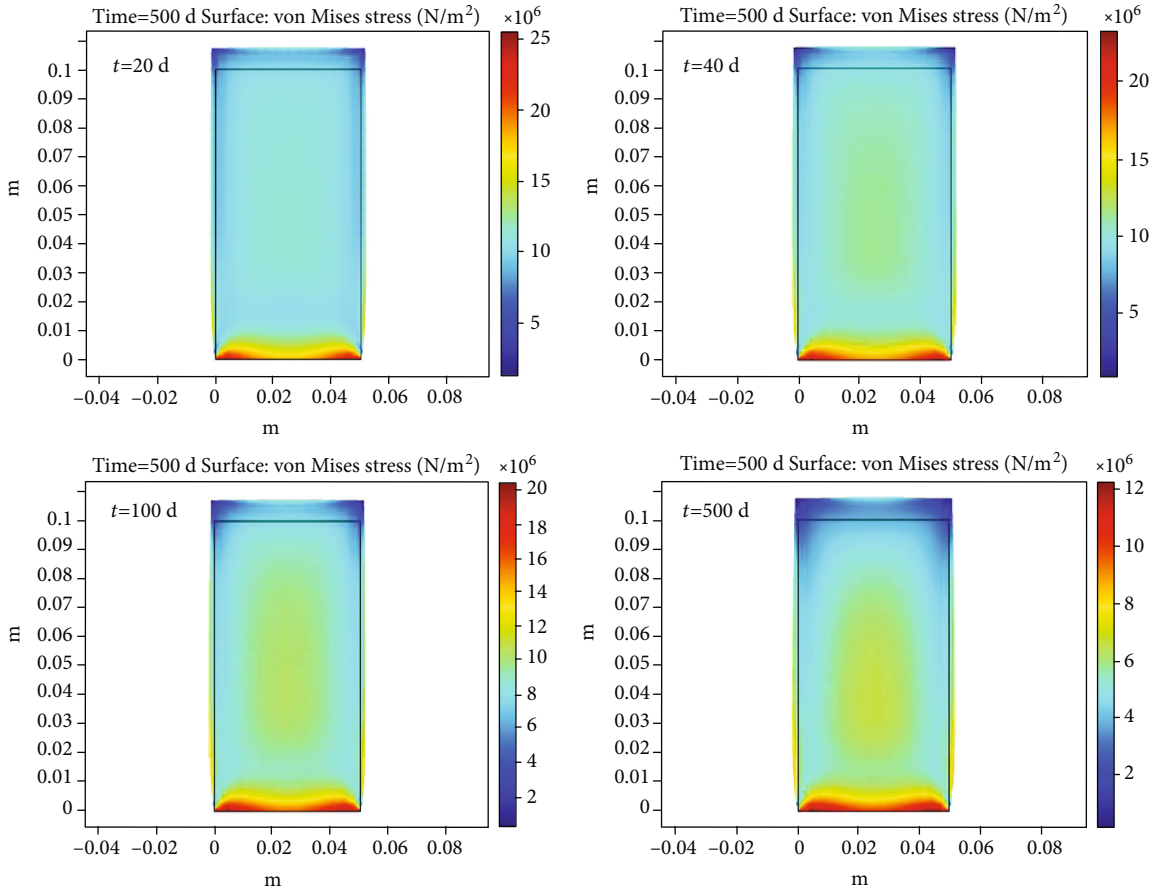
FIGURE 5: Evolution of stress distribution in coal.

constant (ε_L), the volume expansion degree of pores and fractures in coal seam increases, new pores and fractures are produced, and the fractal dimension of coal seam also increases.

5. Influences of Structural Parameters on Permeability

In this paper, based on the fractal geometry method, a dual pore seepage coupling model is established, in which the maximum fracture length, the fractal dimension of fracture length, the fractal dimension of pore size, and the fractal dimension of pore throat tortuosity are mainly considered, and the proposed model does not contain empirical parameters.

5.1. Influence of Fractal Dimension of Fracture Length. Under the influence of adsorption stress and in situ stress, we calculated the change of coal permeability with the fractal dimension of coal fracture length. Figure 15 shows the difference results between the fractal model established in this paper and the classical cubic model. When the number of fractures is constant, the two-scale fractal model established in this paper increases the permeability of coal seam with the increase of fractal dimension of fracture length. This cannot be obtained in the classical cubic model.

Because of the two-dimensional model, the fractal dimension is a fraction between 1 and 2. The closer the fractal dimension is to 2, the longer the fracture length span is, that is, the larger the number of large-scale fractures is. According to Figure 15, the closer the fractal dimension is to 2, the higher the permeability of coal seam is, which is consistent with the actual seepage situation of coal seam. When the fractal dimension of fracture is 1.9, the permeability is about 55% different from that before the change.

5.2. Influence of Maximum Fracture Length. Under the same conditions, the mechanism of coal permeability varying with the maximum fracture length is discussed, as shown in Figure 16.

As shown in Figure 16, with the increase of maximum fracture length, the permeability of coal seam increases gradually. It is well known that the size of fracture is much larger than that of throats and pores. Therefore, the more fracture gas flows through, the less small-scale structures such as pore and throat experienced, and the smaller the resistance to flow. Therefore, when the fractal dimension, pore size, and other microstructure parameters are unchanged, the average size of gas migration channel increases with the increase of the maximum fracture length, the flow resistance of gas decreases, and the permeability increases. However, in the classical cubic model, the influence of this factor on macropermeability is usually neglected.
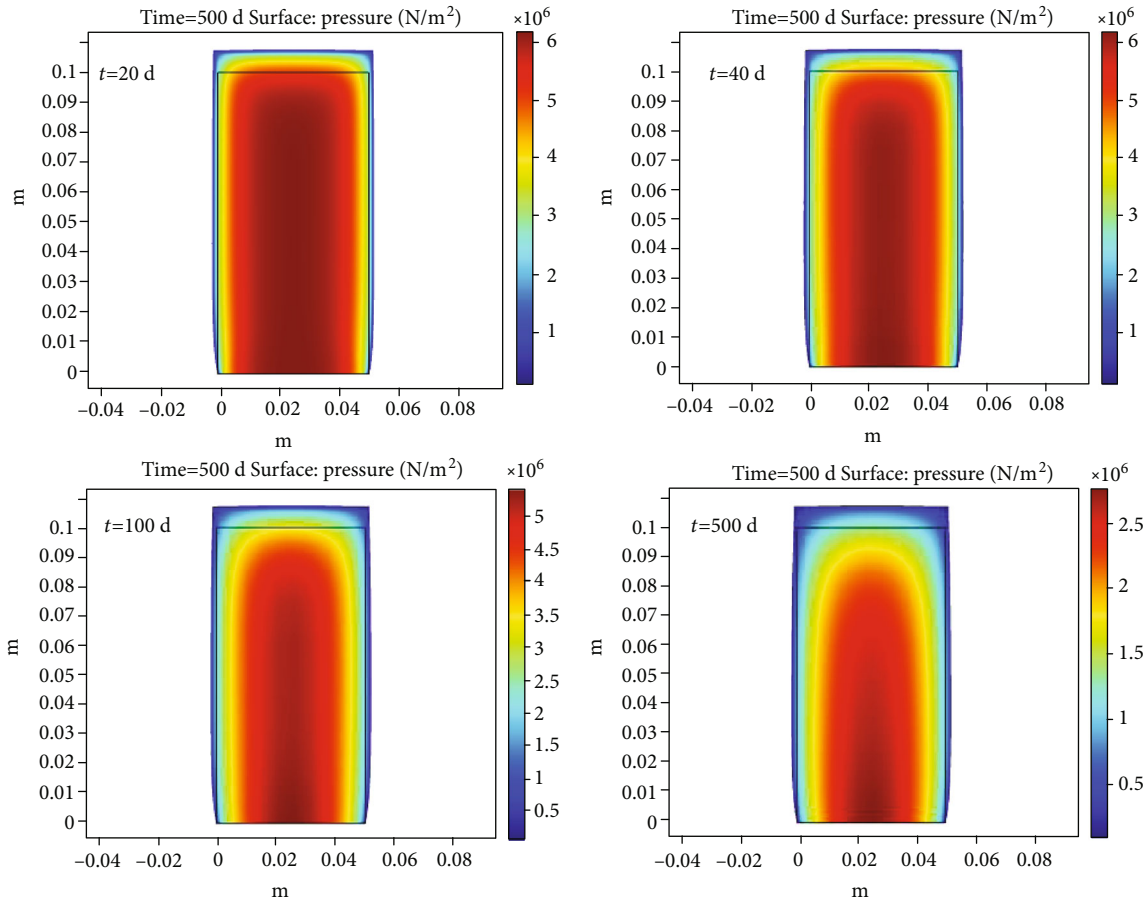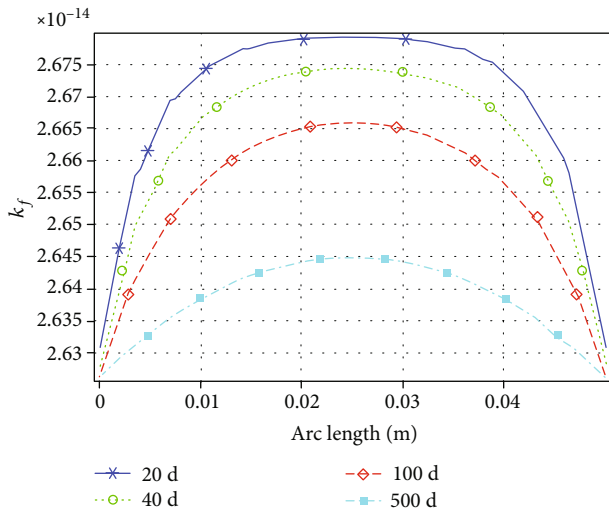
FIGURE 6: Evolution of pore pressure.

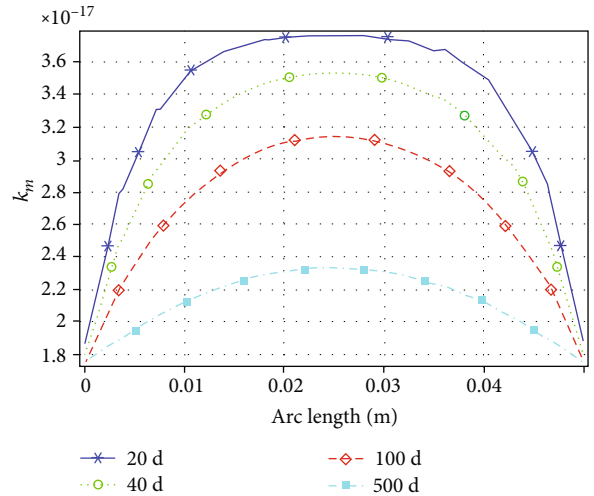FIGURE 7: Evolution of permeability in the upper boundary fracture system.

FIGURE 8: Evolution of permeability in the upper boundary pore system.

5.3. Influence of Fractal Dimension of Throat Diameter.

Similarly, we studied the change of permeability of the coal pore system with the fractal dimension of throat diameter. The two-scale fractal seepage model and the classical cubic model are presented in this paper. The trend diagram of the influ-ence of pore fractal dimension on permeability is shown in Figure 17.

From Figure 17, it can be seen that in the two-scale fractal seepage model established in this paper, with the increase of fractal dimension of throat diameter, the permeability of the
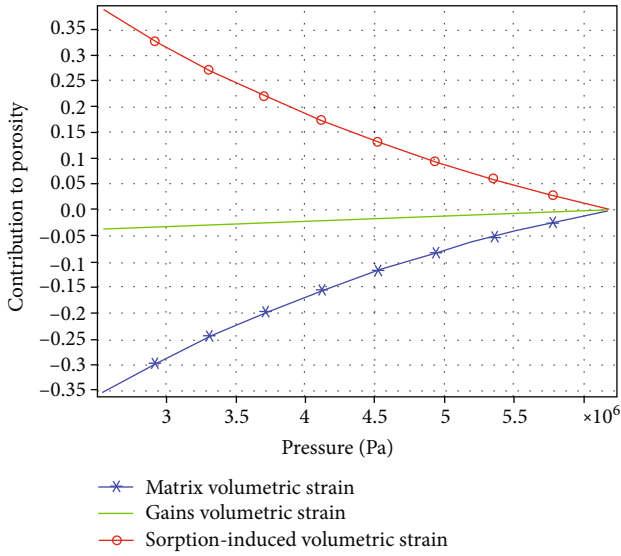
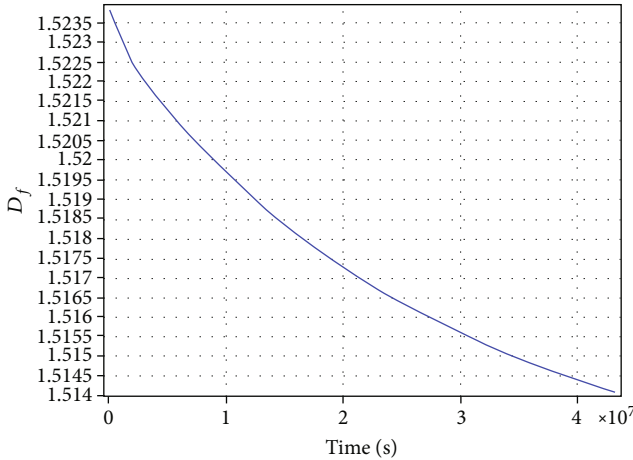Figure 9: Effect of adsorption strain and volume strain on porosity.

Figure 10: Evolution of the fractal dimension of fracture length at the location (0.025, 0.05) by the fractal model.
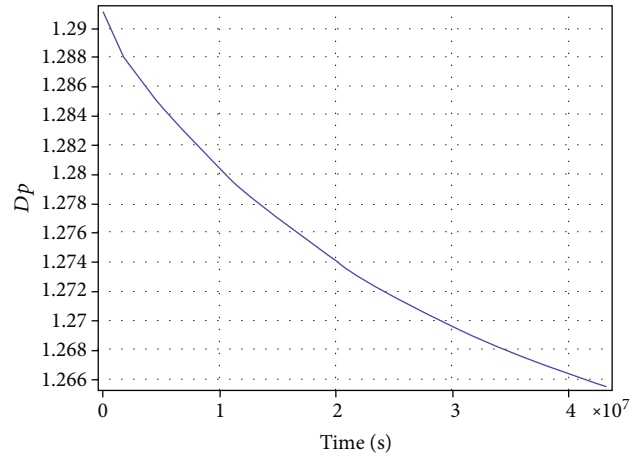

Figure 11: Evolution of the fractal dimension of throat diameter at the location (0.025, 0.05) by the fractal model.

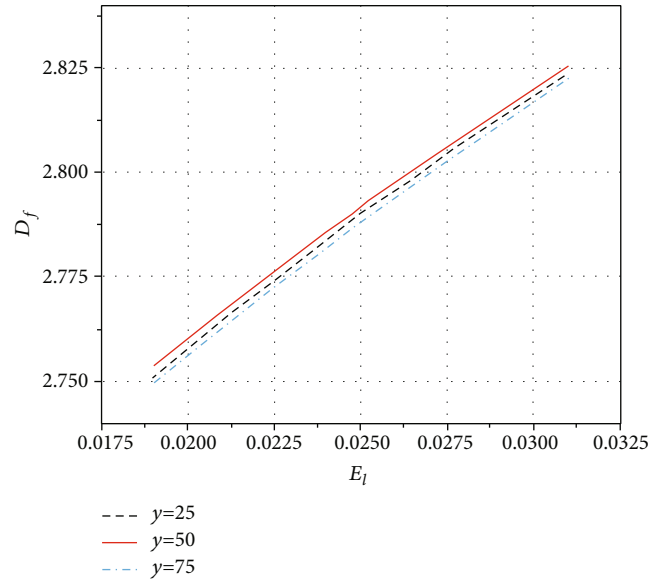Figure 12: Influence of Langmuir volume strain constant ε_L on the fractal dimension D_f of fracture length.

coal pore system also shows an increasing trend. In the two-dimensional structure, with the increase of pore fractal dimension, the larger the number of large diameter throats, the smaller the flow resistance. Therefore, in this model, with the increase of pore fractal dimension, the higher the coal pore coverage, the greater the permeability of the coal pore system. This is beyond the description of the classical cubic model.

5.4. Influence of Fractal Dimension of Throat Tortuosity. The variation of permeability of the coal pore system under different throat fractal dimension is shown in Figure 18. It shows that in the two-scale fractal model, with the increase of fractal dimension of throat tortuosity, the permeability of coal seam decreases gradually.

In this study, a two-dimensional model is used. The fractal dimension of the larynx is between 1 and 2. The closer to 2, the greater the curvature of the larynx and the greater the resistance of the gas flow process. Therefore, with the

increase of fractal dimension of throat, the permeability of the coal pore system shows a downward trend. With the change of the fractal dimension of the larynx, the difference of solution increased, so the new fractal model is closer to the real situation than the classical cubic model. It can be seen that although the fractal dimension of pore and throat directly affects the permeability of the whole model, the order of magnitude is much smaller than the fractal dimension and maximum fracture length at the fracture scale. Therefore, the pore size structure parameters have little influence on the overall permeability of coal samples.

6. Conclusion

In this study, a new two-scale stress-flow fractal model is established, which combines gas flow, adsorption, and desorption with coal deformation process, and then quantitatively
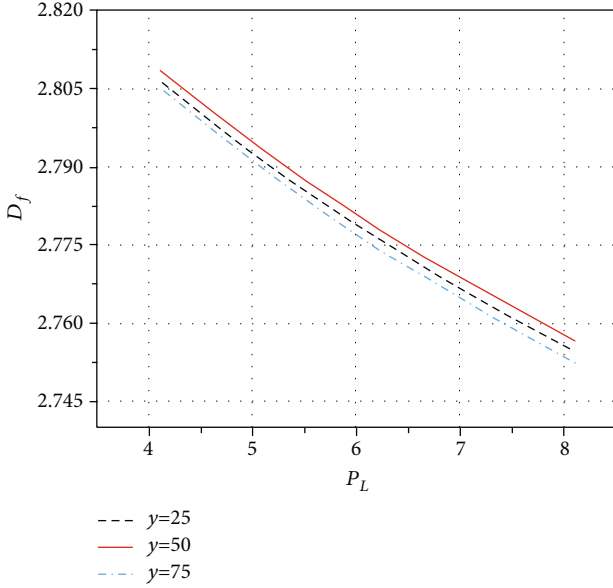
--- $y=25$
— $y=50$
-·- $y=75$

FIGURE 13: Influence of Langmuir pressure constant P_L on the fractal dimension D_f of fracture length.

--- $y=25$
— $y=50$
-·- $y=75$
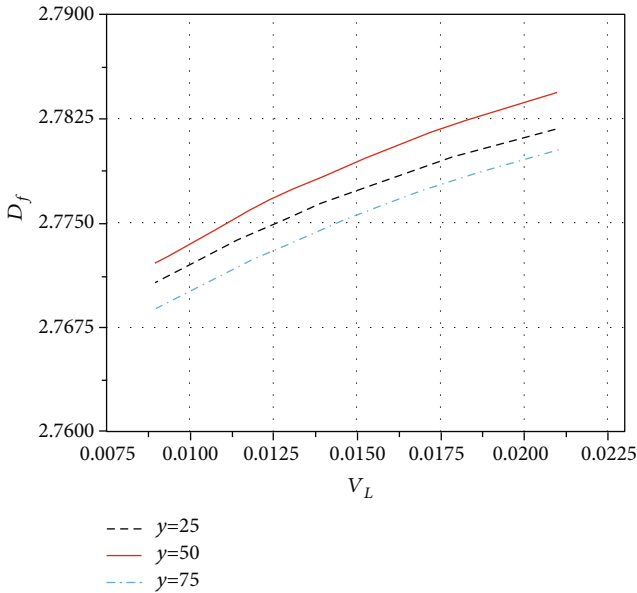
FIGURE 14: Influence of Langmuir volume constant V_L on fracture length fractal dimension D_f.

■ Dual-fractal model
■ Cubic law model

FIGURE 15: Permeability evolution under different fractal dimension of fracture length.

■ Dual-fractal model
■ Cubic law model
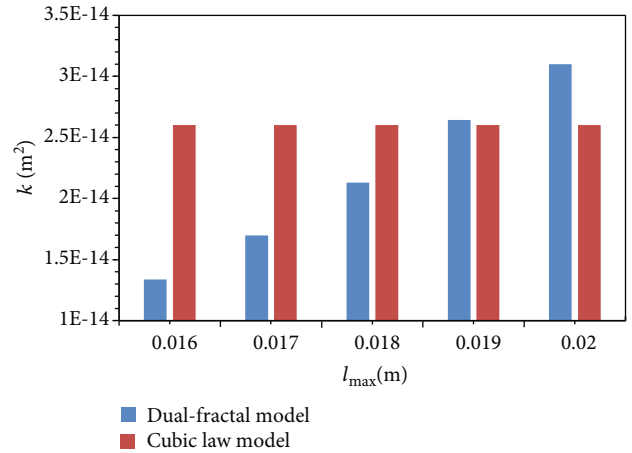
FIGURE 16: Permeability evolution under different maximum fracture length.

analyzes the influence of structural parameters such as coal fracture, pore, and throat on coal permeability. The classical model is based on the relationship between porosity and permeability, while the model proposed in this paper can consider the influence of fracture pore structure parameters on permeability under multifield coupling. Based on the numerical simulation results mentioned above, the following conclusions can be drawn:

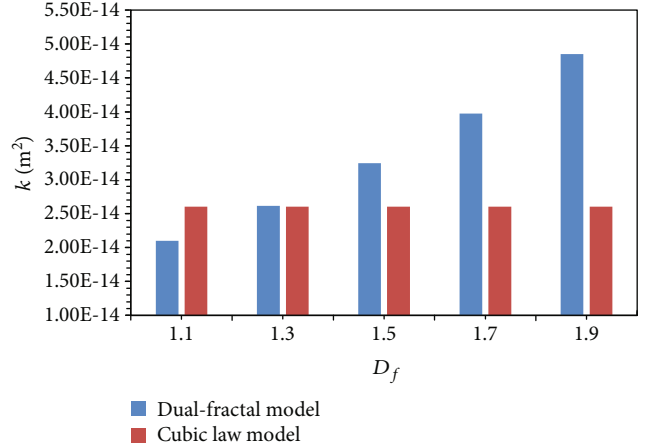(i) The effects of four parameters characterizing microstructure on coal permeability are discussed: (1) fractal dimension of throat diameter, (2) fractal dimension of throat tortuosity, (3) maximum fracture length, and (4) fractal dimension of fracture length. Permeability is directly proportional to fractal dimension of fracture length, maximum fracture length, and throat diameter and inversely proportional to fractal dimension of throat tortuosity

(ii) Among the four parameters used in characterization, fracture structure parameters have a greater impact on permeability, while pore scale structure parameters have a smaller impact on overall permeability. From the sketch figure of permeability and structural parameter evolution of the classical cubic model, we can conclude that the fracture-pore structure is an indispensable factor in the physical evolution of coal seam from the initial state to the final equilibrium state

(iii) Under the simulation parameters in this paper, with the passage of time, the stress in the central gas-carrying area of coal increases gradually, and the deformation of coal increases gradually; the stress
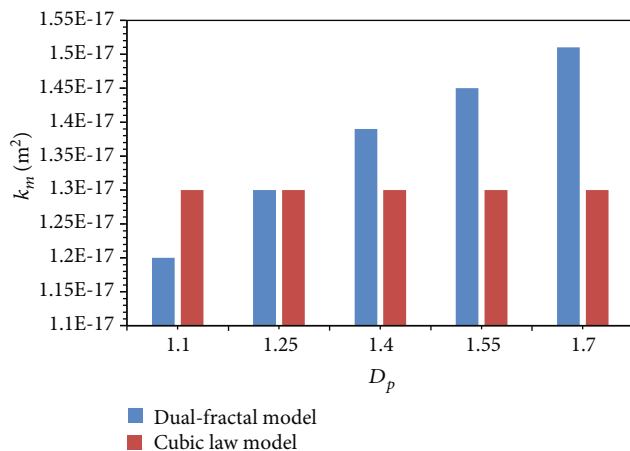
Figure 17: Permeability evolution under different fractal dimension of throat diameter.
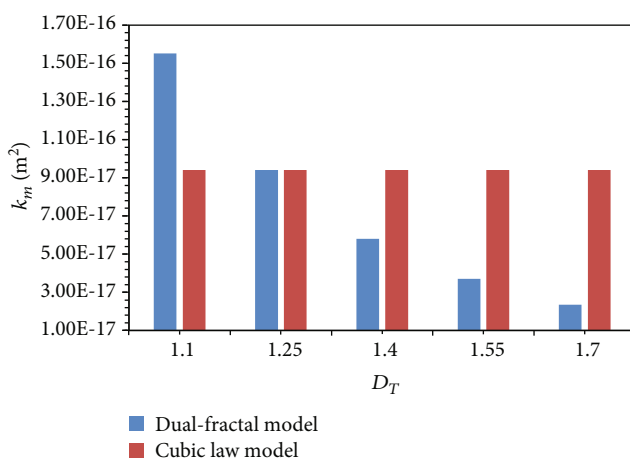

Figure 18: Permeability evolution under different fractal dimension of throat tortuosity.

at the bottom increases gradually, and the stress at the top decreases gradually; the pore pressure decreases gradually from the top, left, and right to the center, while the pore permeability of the top fracture decreases as a whole

Data Availability

The data related to the submission is available.

Conflicts of Interest

The authors declare that they have no conflicts of interest.

Acknowledgments

References

[1] F. Arand and J. Hesser, "Accurate and efficient maximal ball algorithm for pore network extraction," *Computers & Geosciences*, vol. 101, pp. 28–37, 2017.

[2] B. Bauer, X. Cai, S. Peth, K. Schladitz, and G. Steidl, "Variational-based segmentation of bio-pores in tomographic images," *Computers & Geosciences*, vol. 98, pp. 1–8, 2017.

[3] X. Zhao, *The study of reconstruction method of digital core and pore network model*, China Petrol Univ (East China), 2009.

[4] M. Starnoni, D. Pokrajac, and J. E. Neilson, "Computation of fluid flow and pore-space properties estimation on micro-CT images of rock samples," *Computational Geosciences*, vol. 106, pp. 118–129, 2017.

[5] P. E. Øren and S. Bakke, "Process based reconstruction of sandstones and prediction of transport properties," *Transport in Porous Media*, vol. 46, no. 2/3, pp. 311–343, 2002.

[6] A. Q. Raeini, B. Bijeljic, and M. J. Blunt, "Generalized network modeling: network extraction as a coarse-scale discretization of the void space of porous media," *Physical Review E*, vol. 96, no. 1, article 013312, 2017.

[7] A. Hajizadeh, A. Safekordi, and F. A. Farhadpour, "A multiple-point statistics algorithm for 3D pore space reconstruction from 2D images," *Advances in Water Resources*, vol. 34, no. 10, pp. 1256–1267, 2011.

[8] K. Liu, M. Ostadhassan, J. Zhou, T. Gentzis, and R. Rezaee, "Nanoscale pore structure characterization of the Bakken shale in the USA," *Fuel*, vol. 209, pp. 567–578, 2017.

[9] Y. Ju, J. Zheng, M. Epstein, L. Sudak, J. Wang, and X. Zhao, "3D numerical reconstruction of well-connected porous structure of rock using fractal algorithms," *Computer Methods in Applied Mechanics and Engineering*, vol. 279, pp. 212–226, 2014.

[10] R. C. Liu, Y. J. Jiang, B. Li, and X. Wang, "A fractal model for characterizing fluid flow in fractured rock masses based on randomly distributed rock fracture networks," *Computers and Geotechnics*, vol. 65, pp. 45–55, 2015.

[11] T. Miao, A. Chen, L. Zhang, and B. Yu, "A novel fractal model for permeability of damaged tree-like branching networks," *International Journal of Heat and Mass Transfer*, vol. 127, pp. 278–285, 2018.

[12] M. R. Deinert, J. Y. Parlange, and K. B. Cady, "Simplified thermodynamic model for equilibrium capillary pressure in a fractal porous medium," *Physical Review E*, vol. 72, no. 4, article 041203, 2005.

[13] M. R. Deinert, A. Dathe, J. Y. Parlange, and K. B. Cady, "Capillary pressure in a porous medium with distinct pore surface and pore volume fractal dimensions," *Physical Review E*, vol. 77, no. 2, article 021203, 2008.

[14] P. Xu and B. Yu, "The scaling laws of transport properties for fractal-like tree networks," *Journal of Applied Physics*, vol. 100, no. 10, article 104906, 2006.

[15] P. Xu, B. Yu, M. Yun, and M. Zou, "Heat conduction in fractal tree-like branched networks," *International Journal of Heat and Mass Transfer*, vol. 49, no. 19-20, pp. 3746–3751, 2006.

[16] P. Xu, B. Yu, Y. Feng, and Y. Liu, "Analysis of permeability for the fractal-like tree network by parallel and series models," *Physica A: Statistical Mechanics and its Applications*, vol. 369, no. 2, pp. 884–894, 2006.

[17] T. Ishibashi, N. Watanabe, N. Hirano, A. Okamoto, and N. Tsuchiya, "Beyond-laboratory-scale prediction for channeling flows through subsurface rock fractures with heterogeneous aperture distributions revealed by laboratory evaluation," *Journal of Geophysical Research: Solid Earth*, vol. 120, no. 1, pp. 106–124, 2015.

[18] A. Costa, "Permeability-porosity relationship: a reexamination of the Kozeny-Carman equation based on a fractal pore-space geometry assumption," *Geophysical Research Letters*, vol. 33, no. 2, pp. 87–94, 2006.

[19] L. Guarracino, "A fractal constitutive model for unsaturated flow in fractured hard rocks," *Journal of Hydrology*, vol. 324, no. 1-4, pp. 154–162, 2006.

[20] T. J. Miao, B. M. Yu, Y. G. Duan, and Q. Fang, "A fractal analysis of permeability for fractured rocks," *International Journal of Heat and Mass Transfer*, vol. 81, pp. 75–80, 2015.

[21] T. Miao, S. Yang, Z. Long, and B. Yu, "Fractal analysis of permeability of dual-porosity media embedded with random fractures," *International Journal of Heat and Mass Transfer*, vol. 88, pp. 814–821, 2015.

[22] T. J. Miao, S. J. Cheng, A. M. Chen, and B. Yu, "Analysis of axial thermal conductivity of dual-porosity fractal porous media with random fractures," *International Journal of Heat and Mass Transfer*, vol. 102, pp. 884–890, 2016.

[23] Y. Wu, J. Liu, D. Elsworth, H. Siriwardane, and X. Miao, "Evolution of coal permeability: contribution of heterogeneous swelling processes," *International Journal of Coal Geology*, vol. 88, no. 2-3, pp. 152–162, 2011.

[24] J. D. N. Pone, M. Hile, P. M. Halleck, and J. P. Mathews, "Three-dimensional carbon dioxide-induced strain distribution within a confined bituminous coal," *International Journal of Coal Geology*, vol. 77, no. 1-2, pp. 103–108, 2009.

[25] G. Liu, J. Liu, L. Liu, D. Ye, and F. Gao, "A fractal approach to fully-couple coal deformation and gas flow," *Fuel*, vol. 240, pp. 219–236, 2019.

[26] P. Cao, J. Liu, and Y. K. Leong, "Combined impact of flow regimes and effective stress on the evolution of shale apparent permeability," *Journal of Unconventional Oil and Gas Resources*, vol. 14, pp. 32–43, 2016.

[27] C. Wang, J. Liu, J. Feng, M. Wei, C. Wang, and Y. Jiang, "Effects of gas diffusion from fractures to coal matrix on the evolution of coal strains: experimental observations," *International Journal of Coal Geology*, vol. 162, pp. 74–84, 2016.

[28] A. Mitra, S. Harpalani, and S. Liu, "Laboratory measurement and modeling of coal permeability with continued methane production: Part 1 - Laboratory results," *Fuel*, vol. 94, no. 1, pp. 110–116, 2012.

[29] J. Chen, B. Yu, P. Xu, and Y. Li, "Fractal-like tree networks increasing the permeability," *Physical Review E*, vol. 75, no. 5, article 056301, 2007.

[30] S. Zhang, J. Liu, M. Wei, and D. Elsworth, "Coal permeability maps under the influence of multiple coupled processes," *International Journal of Coal Geology*, vol. 187, pp. 71–82, 2018.